APPLICATION OF DIFFERENT FAILURE CRITERIA IN FUEL PIN MODELLING AND CONSEQUENCES FOR OVERPOWER TRANSIENTS IN LMFBRs

B. KUCZERA, P. ROYL

Institut für Reaktorentwicklung,
Kernforschungszentrum Karlsruhe, D-7501 Leopoldshafen, Germany

SUMMARY

The CAPRI-2 code system for analysis of hypothetical core disruptive accidents in LMFBRs has recently been coupled with the transient deformation model BREDA-2. The new code system determines thermal and mechanical loads under transient conditions for both, fresh and irradiated fuel and cladding, taking into account fuel restructuring as well as effects from fission gas and fuel and clad swelling. The system has been used for analysis of mild uncontrolled overpower transients in the SNR-300 to predict failure, and to initialize and calculate subsequent fuel coolant interaction (FCI). Thirteen channels have been coupled by point kinetics for the whole core analysis. Three different failure mechanisms and their influence on accident sequence have been investigated:

1. Clad melt-through;
2. Clad burst caused by internal pressure build-up;
3. Clad straining due to differential thermal expansion between fuel and clad cylinders.

Melt-through of cladding was predicted from a threshold value for peak fuel melt fraction. Clad burst and clad straining failures were determined from BREDA-2 deformation analysis by comparing calculated loads with axially dependent ultimate stresses and strains of the cladding material, respectively.

Melt-through of cladding takes place mainly in fresh fuel, where burst and straining failure are unlikely to occur because of the fabricated fuel-clad gaps and small gas contents in the fuel. Melt-through is always predicted prior to significant build-up of fuel vapor pressures. Failure is usually assumed at peak power position. Failure by internal pressure build-up is caused by rather high cavity pressures, which are between 500 and 1500 atm. Fill and fission gas release to the cavity coupled with fuel density changes upon melting are the main sources for pressure increase. Failure position is predicted slightly above peak power point. Failure by clad straining is mainly determined by pre-transient gapsize distribution and fluence dependent high temperature embrittlement of the cladding material with brittle mode failure occurring near the top and ductile mode failure around midplane of the pin.

While the burst criterion predicts earlier failure for low powered high irradiated fuel due to the higher fission gas content, the rupture strain criterion yields an earlier failure for high powered high irradiated pins due to larger high temperature embrittlement of cladding. Applying both failure mechanisms in accident analysis of the high irradiated core leads to milder accident sequences than in a medium burnup core in particular when considering reactivity feedback due to fuel sweep-out.

The results of these analyses show that each failure mechanism will lead to rather different failure and accident sequences. There is still a lack of experimental data from which failure thresholds can be derived. To get better predictions from the applied models an improved understanding of fission gas release and its relation to fuel porosity also some better experimental data on fluence and temperature dependent rupture strains of the cladding material should be available.

1. Introduction

For analysis of hypothetical core disruptive accidents (HCDAs), failure time and failure position of a fuel pin in connection with the state of the fuel itself are important parameters with respect to the initial conditions of the following fuel coolant interaction (FCI). Various criteria to determine fuel pin failure have been derived both for fresh and irradiated pins on an experimental or theoretical basis and are published in literature. This paper will compare different criteria for failure mechanisms of irradiated fuel by investigating their influence in an overpower transient. Special considerations will be given to the resulting FCI, failure sequences and to the potential for an early shutdown.

To the organization of this contribution: After a short description of the used computer models, the operating conditions of the reactor are outlined, followed by the definition of the considered accident in connection with the applied failure criteria. Then the results of the chosen base case are discussed with more detail. Results of parametric cases are discussed next and will be referred to this base case for comparison.

2. Applied Computer Models

Calculations of the overpower transient up to failure were carried out with the integrated CAPRI-II/BREDA-II [1,2] system. The accident sequence after pin failure in particular the influence of fuel coolant interaction and fuel sweepout effects was then simulated with the HOPE code [3]. The fuel conditions at failure as determined by the BREDA-II deformation analysis were supplied as input to the HOPE simulations.

2.1 CAPRI-II/BREDA-II Model

The CAPRI-II system [1] used for the simulation of the transient core behavior during the pre-disassembly phase is based on single deterministic models. Particular effects of thermohydraulics and neutron kinetics of the core can be described within a multi-subassembly arrangement of up to 30 characteristic channels. Each channel represents a characteristic fuel pin from a group of subassemblies surrounded by equivalent coolant and structural materials. A detailed multi-bubble slug ejection model BLOW-3 [11] allows to take sodium boiling events into account. Thermal and mechanical loads on the fuel pin resulting from transient accident conditions are calculated by the deformation model BREDA-II. The characteristic channels are coupled by point kinetics with axial and channel dependent power shape - and reactivity worth distributions for coolant and fuel and for the Doppler feedbacks from the different subassembly groups represented by the channel. These distributions are regarded independent of time.

The mechanical analysis of the fuel pin in BREDA-II [2] is based on the plane strain approximation of the theory of thermal elasticity. The solid fuel is treated as a material with elastic strength properties, while the

rheological model for the cladding tube is based on an elastic, ideal plastic material. Appropriate mesh configurations (up to 20 axial pin segments and 10 axis-symmetric, radial fuel nodes) permit the description of space dependent long-term and short-term modifications of the fuel pin. Steady-state fuel restructuring and fuel and clad swelling are taken into account and change the geometry of the pin. The pressure in the pin is increased during steady-state by partial fission gas release. During power excursion, transient fuel swelling and pressure increase in the central void due to transient fission gas behavior are included in the deformation analysis. Clad failure depends on the application of various failure criteria, which will be discussed in chapter 4.

2.2 HOPE-Model

The HOPE "Hypothetical Overpower Excursion" Model [3] has been developped in particular to simulate the events following a fuel pin failure in an overpower accident, i.e. the molten fuel and fission gas ejection from the fuel cavity into the coolant channel, thermal fuel coolant interactions and the resulting coolant void and fuel motion feedbacks. HOPE is an integral multi-channel code like the CAPRI-system, whose input is consistently set up by CAPRI-II. Steady-state phenomena,in particular fuel restructuring and burn up dependent fission gas concentration in the fuel and pressure in the fuel pin cavity are calculated consistently with BREDA-II. The failure conditions (for instance failure melt fraction and failure position) evaluated by BREDA-II for different characteristic fuel pins can be used in the HOPE simulation to initiate failure events. Point kinetics coupling of different channels is performed within HOPE with feedbacks calculated from the shape functions provided by CAPRI-II.

HOPE has a rather refined model to describe fragmentation of the ejected fuel, which leads to rapid variations in fuel sodium heat transfer, but due to a lack of corresponding experimental data instantaneous fragmentation has been assumed for these investigations.

3. Description of the Reactor

An uncontrolled reactivity accident was simulated for a large end of life (EOL) core, which is similar to the MARK 1A core of the SNR-300.

3.1 Characteristic Data and Operating Conditions of the Reactor

Fig.1 gives a rough sketch of this reactor and its setup for the accident simulations. The core is represented by 13 characteristic channels with associated concentric core rings for each channel being marked.Nine channels were used to simulate the inner core zone. The outer core zone with a higher Pu-enrichment and the radial blanket region are represented by two channels each. Axially the height from the lower pin attachment to the upper subassembly exit has been divided into 29 meshes, 20 of them are used for the axial core blanket region.

The reactor operates at a steady-state power of 762 MW, which is achieved with a maximum linear heating rate of 290 W/cm. The assumed EOL core with 441 days operating time has rather flat axial and radial power shapes, which will strongly promote failure coherence in the ramp type accident. Fig.2 shows the radial power distribution at the core mid-plane. Channel 10, the innermost ring of the higher enriched core zone has nearly the same maximum power density as the central channel. One should note, however, that the fast neutron flux (E >0.1 MeV), which is also plotted in this figure is significantly smaller in this region. Thus flux to power ratio, which is important for the BREDA-II calculated gap size variations due to differential fuel and clad swelling has a minimum in this channel.

The core has a rather high positive coolant void coefficient of 5.5 $, and as Fig.1 shows voiding of the inner core regions leads to positive feedbacks in all except the outermost coolant channel. With sodium in a Doppler coefficient of -0.9 $ is calculated per 1000°C temperature rise. Complete removal of sodium will half this value, so that core voiding will reduce the Doppler coefficient.

3.2 Steady-state Characterization of a Fuel Pin

Determination of the steady-state condition of the reactor is an iterative procedure in CAPRI-II. Starting with a full cylinder configuration of the fuel column the first estimation of the temperature field enables to calculate the fuel restructuring pattern in a rough way. A recalculation which takes into account the evaluated changes in pin geometry as well as the resulting variations of radial distributions of fuel porosity and power density is repeated until a convergence criterion derived from temperature distribution is fulfilled. The data, which are relevant for this characterization, and some results are given in Tab.I.

Fig.3 compares the calculated results for two representative high and low powered fuel pins with same operating times. In channel 9 the maximum linear rod power is 245 W/cm, in channel 10 the corresponding value amounts to 285 W/cm, which results in peak burnups of 66200 and 76500 MWd/tM.

Restructuring, which is calculated by a three region model with restructuring isotherms and reduced fuel porosities from Tab.I, is rather different in these channels. As shown in Fig.3 only the high powered pin is calculated to have a columnar grain-growth region. Due to the higher columnar grain density this results in a larger central void volume for this channel, which is also important for the transient pressure buildup in the fuel pin cavity.

Steady-state fission gas release was determined from Ref. [5]. Assuming pressure equilibrium with the lower fission gas plenum, gas release results in a cavity pressure of 24 bar in channel 9 and due to the higher gas production and release a value of 33 bar is calculated for channel 10. These values cover also the range achieved in other channels. Volume and pressure of the central void and the fission gas, which is mainly retained in the

unrestructured fuel regions, will be shown to be important parameters besides power distribution, which determine the failure sequence.

Fuel swelling due to gaseous and solid fission products is estimated as a function of burnup by the linear swelling coefficient from Tab.I and partly compensated by porosity reduction in the different fuel regions [2]. Axial peak power position determines the point of maximum fuel swelling.

Contrary to the fuel the reason for clad swelling is mainly the formation of pores in the cladding material, which depends on the cladding temperature and the time integral of the fast neutron flux [6]. The flux to power ratio strongly influences differential fuel and clad swelling. This ratio is smallest in channel 10, which is the reason why steady-state gap closure in channel 10 is calculated almost over the whole active core length.

4. Case Definition

The influence of failure criteria was investigated in an overpower accident with a mild reactivity insertion ramp of 15 ¢/sec. This ramp would be achieved by coherent withdrawal of all control rods of SNR-300 with maximum velocity.

In the definition of clad failure criteria the problem arose to associate dominant failure reasons and mechanisms with characteristic threshold values, which can be approximately quantified and calculated by methods of fuel pin deformation models. If those values are available, it is possible to obtain failure time and position from transient load conditions of the fuel pin.

With respect to failure reasons in this mild overpower transient the following symptoms are considered important:

1. mechanical fuel-clad-interaction due to differential expansion,
2. clad loading due to fission gas pressure,
3. local contact with molten fuel.

From material properties of the cladding tube four phenomenological failure modes are derived:

a) ductile fracture
b) brittle fracture
c) high strain rate burst fracture
d) loss of tensile properties at high temperatures.

The selected failure thresholds to simulate the above mentioned failure mechanisms and failure modes are listed in Tab.II. Each criterion has been defined as a separate case with a number, which will be referred to in the later discussion:

1. In setting up criteria for the differential thermal expansion failure mechanism values of rupture strain for ductile and brittle mode failure were derived from data found in the literature. The definition

of these values for irradiated material is difficult, since tensile properties of cladding depend on fluence, temperature and loading rate.

In case C1 the equivalent rupture strain has been assumed to be 1%. The small value reflects the ductility decrease due to steady-state irradiation. In case C2 loss of ductility due to Helium embrittlement depends on fluence and on the temperature level for high temperature embrittlement. From experimental results [7] it was estimated that above cladding temperatures of 670°C rupture of the tube will occur, when the plastic strain reaches a fluence dependent threshold value. This was assumed to decrease from 0.007 to 0.001 in the fluence range of 10^{22} to 10^{23} n/cm^2 (E>0.1 MeV). Its smallest value is thus achieved in the central channel. In both cases C1 and C2 a strain rate dependency of failure thresholds was neglected.

2. Clad loading due to fission gas pressure was assumed to cause a high strain rate burst failure mode. The temperature dependent rupture stress [8] was used as failure threshold for the so called burst pressure criterion (case C3). Loading of the clad is calculated through loading of the strengthless fuel by reducing the transient cavity pressure with the ratio of local melt and inner cladding radius.

3. Without explicitly relating them to any failure mode two additional thermal failure criteria from the literature [9,10] were used to simulate two combined mechanisms, failure due to fission gas pressure and due to local clad contact with molten fuel. The unrestructured fuel melt criterion (case C4) predicts failure when the first unrestructured fuel node reaches the solidus. The melt fraction criterion (case C5), which is mainly derived from TREAT experiments, predicts failure, when the peak fuel melt fraction exceeds a value of 30%. Both criteria shall simulate the thermodynamic state of the fuel at which high rates of fission gas release and pressure rises in the cavity are expected. Axial failure position for both thermal criteria are all assumed at the peak power position.

The pressure in the fuel pin cavity is an important quantity both for determining fuel pin failure and for initiating the subsequent FCI. Starting from steady-state values its variations are calculated taking into account transient fission gas release and fuel density changes upon melting. Most of the retained fission gas (90%) was assumed to be released at fuel melting. Since restructured fuel fission gas content was small, rapid pressure rises were calculated only after the melt radius reached the unrestructured fuel regions.

The BREDA-II calculated state of the fuel pin at failure was used within the HOPE code to initiate FCI. A failure rip length of 5 cm was assumed. Fuel and fission gas from the cavity were ejected into the coolant channel according to their time dependent volume fractions. Instantaneous fragmentation of molten fuel into particles of 117 µm was assumed.

Further assumptions made for the HOPE simulations will be discussed under point 5.1 together with the results for case C1, which has been declared to be the base case in these investigations.

5. Results

The transient power histories for the five different cases are compared in Fig.4. In all cases the mild reactivity insertion ramp is soon compensated by negative Doppler feedbacks and power increase becomes rather slow before failure. The high temperature rupture strain criterion (case C2) predicts first failure. Failure points are marked in Fig.4,but as will be discussed failure has no direct influence on reactor power, which is rising at a later time due to sodium boiling through fuel clad heat transfer. In the other four cases fuel pin failure strongly affects the reactor power since the resulting FCI leads to strong sodium void and fuel motion reactivity feedbacks. The two cases C1 and C3 lead to an early shutdown of the reactor while the remaining two cases C4 and C5 with the melt fraction criteria both lead to an energetic core disassembly. Case C1 in which the ductile rupture strain criterion was applied has been declared as base case and will be discussed in the following paragraph with more detail. Following this the influence of the remaining failure criteria will be compared.

5.1 Accident Sequence with the 1 % Ductile Rupture Strain Criterion

Clad failure for a uniform rupture strain of 1% is predicted first in channel 10, the innermost core ring of the outer core zone, which has the smallest flux to power ratio so that differential fuel and clad swelling lead to SS gap closure. Table III summarizes the conditions of channel 10 at failure as determined by the CAPRI-II/BREDA-II calculation. It also gives some characteristic results from the subsequent FCI in this channel and some integral results concerning power and reactivity of the reactor at different points. Results from the FCI and its feedback simulation with the HOPE code are also given in Figs.4 through 7.

Failure is predicted above the axial midplane at 60% active length with only a small fraction of the fuel melted. Unrestructured fuel has not yet reached the solidus and only small amounts of retained fission gas have been released to the cavity so that the cavity pressure has only doubled compared to the SS value. Small failure pressure and small cavity throat area become the major restraints for the time dependent ejection process. Fig.5 shows the mass of molten fuel in the cavity and the amount of fuel injected into the coolant channel together with the time dependent sodium mass in the FCI zone. The injection process for the molten fuel fission gas mixture is calculated from the difference between cavity and FCI zone pressure, which in turn is strongly affected by the composition of the fuel pin cavity and by the fuel to sodium heat transfer and compressibility of the FCI zone. Corresponding cavity and FCI zone pressures after pin failure are given in Fig.6. Failure results in a rapid injection of 60% of the initial mass of molten fuel in the

cavity (Fig.5). The cavity pressure is continuously decreased by removal of the fuel fission gas mixture, while the FCI zone pressure is increased by density changes due to fuel to sodium heat transfer. Due to the applied inertial constraint model for the sodium columns above and below the FCI zone and because of the inertia of the injection process itself the FCI zone pressure shows some strong oscillations initially when the sodium is still in the single phase regime. But rapid rise of sodium temperature and decrease of FCI zone pressure due to slug motion lead to sodium boiling ca. 6 msec after failure. FCI zone pressure and sodium temperature are both coupled after this point, so that fuel to sodium heat transfer leads to a rapid pressure rise, when two phase conditions are met. FCI zone pressure rises above the cavity pressure and further ejections of fuel are cut off. The pressure in the FCI zone reaches a maximum of 48 atm before it is reduced due to the more dominant removal of pressure volume work from FCI zone expansion, by the additional subcooled sodium entering the FCI zone, and due to condensation effects on the colder cladding and structural surfaces. More fuel gets ejected into the FCI zone (Fig.5) when this pressure drops below the cavity pressure, which again causes some rise in FCI zone pressure. But the fraction of molten fuel is continuously decreased in the cavity, the melting rate is too slow to replace all ejected fuel and fuel content in the ejected mixture decreases with ejection time. Besides that sodium mass entering the FCI zone (p.e. as liquid film which is left behind on clad and structural material by the expelled sodium slugs) rapidly reduces the fuel to sodium mass ratio. A maximum ratio of 2.9 is attained after the first injection period, the value decreases by more than 50% after 120 msec FCI time. Large inertias of the liquid sodium slugs and decreasing sodium enthalpy cause some subcooling in the FCI zone and lead to a pressure decrease below the coolant plenum pressure, which causes flow reversal also of the upper liquid slug. The FCI zone volume is decreased, single phase conditions are attained 160 msec after failure, and the old SS coolant flow is rapidly restored. The corresponding FCI zone for this case is plotted in Fig.7 as function of time after failure. The interface positions determine the time dependent voiding and the amount of fuel motion within the coolant channel.

The resulting void and fuel motion feedbacks from this channel are shown in the same graph. They are strongly dependent on failure position. Fuel motion feedback is negative from the beginning, while feedbacks from sodium void are increasing for the first 15 msec after failure until the FCI zone reaches the upper core and blanket regions. The power rises to a maximum of 3.7 times nominal power, then voiding of the negative feedback regions causes some reactivity reductions, so does the upward flow of the lower liquid slug starting some 50 msec after failure. Superposition of void and fuel motion feedback cause a negative reactivity ramp rate ca.15 msec after failure which decreases power and leads to the gradual shutdown of the reactor shown in Fig.8. Fuel sweepout from the active core zone starts shortly after the upper FCI zone interface leaves the active core zone. At this time there is still some

rather strong downward motion of the lower liquid slug so that the sweepout feedback is partially compensated by downward fuel motion towards the core midplane. The transient power descends below SS power ca. 160 msec after failure. At this point the net reactivity is strongly negative and still decreasing due to sweepout.

The results show that with the calculated failure parameters from the 1% ductile rupture strain criterion the overpower accident can lead to an early shutdown, if the sweepout mechanism is effective. As shown in Fig.9 the FCI zone extends from the failure zone till to the top of the subassembly at the shut off point. It is completely filled with subcooled sodium which can provide the required cooling of the fuel columns after shutdown, if one excludes a permanent subassembly plugging due to freezing of ejected fuel.

5.2 Results from the Parametric Cases

Table IV compares the results from the parametric cases with the base case. Applying the high temperature brittle rupture strain criterion in case C2 leads to much earlier failure than in case C1 with failure positions being shifted upwards to 80 - 90 % active height (Fig.9). It is the brittle failure temperature threshold of the cladding material which causes these high failure positions. Channel 6 fails first due to a more rapid rise of coolant temperature. No fuel is molten in the failing channels and the cavity pressures are only slightly higher than at SS. Since the fuel clad gaps are closed in the lower parts of the pins one can neglect any hydraulic coupling of the failure orifice with the lower fission gas plenum. Only some small amount of cavity gas will be puffed into the coolant channel. This effect is assumed negligible. Thus the calculated failure sequence for case C2 which is shown in Fig.4 and Tab.IV has no direct influence on the accident sequence.

The important change brought in by the early brittle failure is that it is likely to prevent further pressure build up in the cavity once a pressure equilibrium with the coolant channel has been established. The assumption for this case was therefore, that molten fuel can enter the coolant channel only after clad melt through. A threshold value of 80% for the peak fuel melt fraction was selected to initiate FCI. But this criterion was not fulfilled before core disassembly. Instead clad coolant heat transfer led to boiling in the sixth channel 9.9 sec after accident initiation. The time of boiling inception is marked in Fig.4. The accident sequence after sodium boiling was described by the BLOW-3 multiple bubble slug ejection model. Due to the large inertia of the liquid sodium slugs and due to the high coolant inlet pressure voiding of the inner core region starts relatively late after boiling inception compared to a flow coast down accident. Therefore, the power rise shown in Fig.4 does not start before 0.8 sec after sodium boiling. But it leads to a rapid core disassembly. Figure 9 shows the void patterns for case C2 at start of core disassembly. Only a small part of the core is voided. The

dominant feedbacks come from voiding of channels 6 and 7. Because a large fraction of the core still contains liquid sodium fuel coolant interactions are likely to occur during the disassembly phase. Thus the high temperature brittle rupture strain criterion leads to an early failure but the accident is terminated rather late by an energetic core disassembly due to sodium voiding.

Application of the burst pressure failure criterion (case C3) leads to a much later failure than in case C1. Channel 11, which represents the outermost core ring with negative void coefficients is the only one predicted to fail. This channel contains low powered fuel with little SS restructuring and a small central void. Fission gas content of unrestructured fuel is rather high, which results in strong transient pressure buildups after fuel melting. A failure pressure of 900 atm is achieved and the peak melt fraction of this channel approaches 30%. The axial failure position (Fig.9) is calculated to be the peak melt fraction position which is ca. 60% of the active core height. A rapid injection of molten fuel takes place after failure. Negative voiding feedbacks and fuel sweepout feedbacks superimpose and lead to a rapid shutdown (Fig.8). When the power drops below the SS value the FCI zone (Fig.9) extends almost over the whole core length with the sodium still being saturated. At this time the net reactivity is negative and still decreasing rapidly. Due to the reduced melting rate further ejections of molten fuel will be small and rapid achievement of single phase conditions is considered likely in this channel provided that frozen fuel will not plug the coolant channel. Thus the burst pressure criterion can lead also to a permanent shutdown of the reactor, this shutdown is achieved here even more rapidly than in the base case C1.

The last two applied failure criteria lead both to rapid and energetic core disassemblies (Fig.8). Calculated failure sequences are rather different however. They are marked in Fig.8 together with the transient power changes after failure. The unrestructured fuel melt criterion (case C4) is met earlier. Channels 4 and 5 fail first closely followed by channel 6. Peak fuel melt fraction in all failed channels is around 20% and cavity pressures are between 80 and 100 atm. Failure sequence is strongly influenced by the SS fuel restructuring. First melting of unrestructured fuel takes place around the lower end of the fuel pin cavity. However, failure position (Fig.9) is assumed to be the point with the highest fuel melt fraction, which is also the point of maximum importance for the resulting reactivity feedbacks. The almost coherent failure of channels 4 through 6 cause strong positive feedbacks due to core voiding and fuel injection. This leads to a rapid power rise which increases the melting rates and causes further injections from the failed channels and failure of new channels. As Fig.8 shows, failures become more and more coherent with increasing power.Transport and injection of fuel towards the peak power position leads to prompt criticality and all remaining core channels fail almost coherently. Core disassembly is initiated about 18 msec after first pin failure, when the maximum average fuel temperature has reached a value of

3200°C. At this time the net reactivity is still increasing at a high rate due to further injections of molten fuel. Because of the rapid power rise due to the coherent failure fuel sweepout could not become effective before core disassembly. As Fig.9 shows the upper FCI zone interfaces from the first failing channels 4 and 5 have not even reached the upper end of the active core zone at onset of disassembly.

Case C5 with the 30% melt fraction criterion leads next to case C3 to the latest failure time. Channels 1 and 2 fail first with cavity pressures around 100 atm. Failure sequence in case C5 is completely determined by the radial distribution of the power density. Compared to case C4 further failures are somewhat delayed relative to the first failing channels (Fig.8). As in case C4 failure positions were assumed around the axial peak melt fraction position. The first failing channels represent a smaller number of subassemblies and feedbacks due to coolant void and fuel injection lead to a more gradual power rise compared with case C4. Fuel sweepout from the active zone of channels 1 and 2 is about to become effective and the power rise has flattened already, when the next channel (10) fails. It is the positive feedback from this channel which prevents an early shutdown. Its voiding and fuel injection again lead to a rapid power rise which causes further injections and failure of additional channels. As in the previous case mainly the feedbacks from fuel injection at the peak melt fraction position leads to prompt criticality. Core disassembly is initiated 40 msec after failure of the first channel with failure having occurred in all core channels. As Fig.9 shows the FCI zone from the first failing channel extends to the coolant mixing plenum. Thus fuel sweepout is effective in these channels, but it is compensated by additional fuel injections due to the increased melting rates. Although the 30% melt fraction criterion leads to a larger failure incoherence between different channels than the unrestructured fuel melt criterion, these calculations show that it will not lead to an early shutdown. In both cases it is mainly the fuel injection at the peak melt fraction position which causes the additional positive fuel motion feedback that leads to prompt criticality. These positions have the highest importance for the resulting feedbacks besides that more time is required to sweep out the fuel compared to the higher failure points from case C1 and C3.

6. Conclusions

As expected the discussed accident sequences show a great sensitivity towards the applied failure criteria. Two criteria, the 1% rupture strain and the burst pressure criterion led to an early shutdown with the shutdown mechanism coming from fuel sweepout. In both cases the reactor is expected to remain subcritical after shutdown since the driving reactivity is likely to be limited in the EOL core to not more than a few dollars. The calculations show that the ejection of molten fuel and the subsequent FCI can be a desired effect to assure fuel sweepout.

Early failures as calculated with the high temperature brittle rupture strain criterion with no molten fuel at failure could not result in an early shutdown but have rather led to core disassembly initiated by core voiding through clad coolant heat transfer. Since there is still no clear experimental evidence as to the magnitude of a possible thermal fuel coolant interaction and since the assumed mechanism of clean sweepout without plateout or plugging has not yet been verified by experiments this accident path might have some larger relevance. When the FCI and fuel sweepout effects are shown by experiments to be less pronounced, sodium boiling through fuel clad heat transfer and voiding of the inner core region would be initiated, so that shutdown will occur during the subsequent disassembly phase.

Energetic accident sequences were calculated with the two thermal failure criteria (cases C4 and C5), which assumed failure location near the peak power node for all channels. When the inner core regions were coherently voided due to FCI fuel sweepout could not become effective before prompt criticality was reached. Instead of sweepout fuel injection into the high importance regions caused the dominant feedbacks in these two cases. Failure sequences in the last two cases were rather different. Melting of unrestructured fuel occurred more coherently than achieving a peak melt fraction of 30% in the different channels. The medium powered pins failed before the high and low powered pins while the melt fraction criterion predicted a failure sequence corresponding to the radial distribution of the peak power density. The assumed coherent failure of all fuel pins within one core ring is a pessimistic assumption. Particularly in a mild ramp, when the pin power at failure is rather low, statistical variations of failure time and position are likely to occur so that fuel sweepout from earlier failed pins might be effective already before failure of additional pins and prevent power to reach the point of instability where more and more channels are beginning to fail. This incoherence effect could be modeled with a larger number of characteristic channels by assuming some statistical variation of the failure thresholds for similar pins. This more refined treatment of fuel failure might lead to an early shutdown also with the last two thermal failure criteria, since the uncertainty band for fuel pin failure will be particularly wide at low melting rates.

The analysis of all irradiation dependent effects has been performed in these simulations by rather simple models. More sophisticated models in particular for SS and transient fuel swelling and fission gas release [12] are available. But it is not efficient to implement these rather time consuming codes in a multichannel system for safety analysis. It is believed more important to calibrate the phenomenological model parameters by SS irradiation experiments and by both out and in pile transients with irradiated fuel. This leads to the more general remark, that these models need to be verified and carefully checked with experiments. One objective of the overpower experiments with irradiated fuel planned in the CABRI reactor [13], is,therefore, the checkout of these applied computer models and the adjustment of their important parameters.

REFERENCES

[1] D.STRUWE,P.ROYL,P.WIRTZ,B.KUCZERA et al.: "CAPRI - A computer code for the analysis of hypothetical core disruptive accidents in the predisassembly phase; CONF-740401-P3

[2] B.KUCZERA: " Simulation of the transient behaviour of LMFBR fuel pins under consideration of special burnup phenomena using the BREDA-II-Model"; Nucl.Eng.Design, Vol.31, No.2, Jan.1975, 294-307

[3] E.T.RUMBLE et al.: "Fuel movement investigations during LMFBR overpower excursions using a new model"; CONF-740401-P3

[4] R.DÜSING et al.:"Analyse hypothetischer Störfälle für den Mark-1A-Kern des SNR 300"; KFK-Report to be published

[5] D.S.DUTT et al.: "A correlated fission gas release model for fast reactor fuels"; Trans.Am.Nucl.Soc. 15 (1), 198 (1972)

[6] K.EHRLICH: "Das Schwellen von Hüll- und Strukturmaterialien unter Neutronenbestrahlung"; Z.Atomwirtschaft, Juli 1971, S.356

[7] D.FAHR et al.: "Post-irradiation tensile properties of annealed and cold-worked type 316 stainless steel"; Proc.BNES Conf.,London,Nov.1972

[8] M.G.STEVENSON et al.: "Effect of reactivity insertion rate on fuel pin failure threshold"; Trans.Am.Nuclear Society,17, p.284 (1973)

[9] L.D.O'DELL et al.: "Failure criteria and failure incoherence"; HEDL 7309-70,4

[10] C.M.COX: "The irradiation performance of uranium-plutonium oxide fuel pins"; Nucl.Safety, Vol.10, No.5, Sept.1969, 380-391

[11] P.WIRTZ: "Ein Beitrag zur theoretischen Beschreibung des Siedens unter Störfallbedingungen in natriumgekühlten schnellen Reaktoren"; KFK-1858, Okt.1973

[12] H.G.BOGENSBERGER, C.RONCHI: "Calculations of the effect of fission gas in a LMFBR, for the analysis of an unprotected overpower transient"; KFK-1990, June 1974

[13] J.BAILLY, G.Kessler, H.J.TEAGUE: "In-pile safety test on fast reactor fuels"; Proc.ENS-Conf.Paris, April 1975

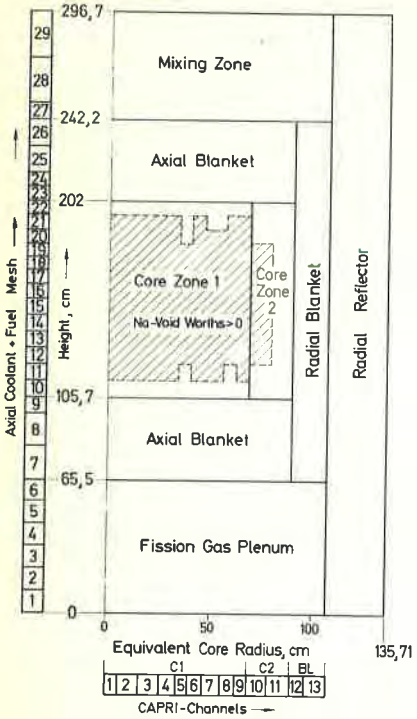

Fig. 1: Core Setup for HCDA Simulations

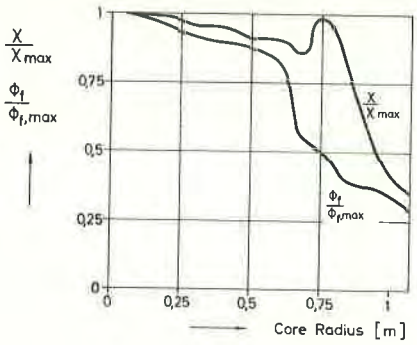

Fig. 2: Radial Power and Flux Distribution at Core Midplane

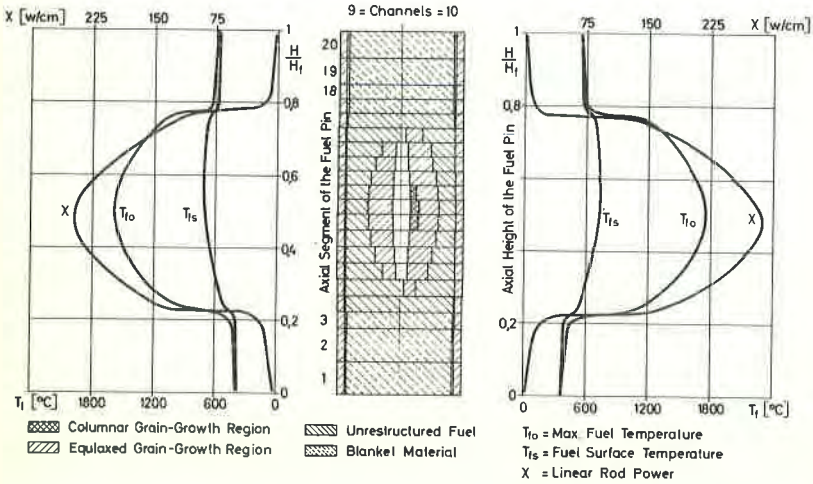

Fig. 3: Steady State Conditions for Low and High Powered Fuel Pins

Tab.I: Data of the fuel pin model

Fuel pin specification

Fuel pellet radius	R_p = 2.55 mm
Inner clad radius	R_{ci} = 2,62 mm
Outer clad radius	R_{co} = 3,00 mm
Fuel material	$(U,Pu)O_2$
Fuel porosity	p = 0.135
Smeared density of the fuel	ρ_s = 0.80 TD
Clad material	Mat. 1.4988

Steady-state operating condition

Maximum linear rod power	χ_{max} = 288 W/cm
Heat conductance of the fuel-cladding gap	h = 0.8 W/cm^2°C
Maximum neutron flux (E > 0,1 MeV)	$\phi_{max} = 3{,}6 \cdot 10^{15}$ n/cm^{2}sec
Operating time	t_{op} = 441 d
Fission gas pressure	p_{fGo} = 24...33 bar

Isotherm for columnar grain-growth region	T_{cg} = 1700 °C
Isotherm for equiaxed grain-growth region	T_{eq} = 1300 °C
Porosity of restructured fuel columnar grain-growth region:	p_{cg} = 0.050
equiaxed grain-growth region	p_{eq} = 0.085
region of unrestructured fuel:	p_{ur} = 0.135
Volumetric fuel swelling factor	v_{sw} = 0.015/at.% burn up
Volumetric clad swelling	see [6]
Steady-state fission gas release	see [5]

Tab.II: Failure criteria applied in various cases and important parameters for subsequent FCI

Case	Failure Criterion	Threshold Value	Failure reason	Failure mode
C1	Ductile rupture strain	plastic strain = 0,01	differential expansion between fuel and clad	ductile mode fracture
C2	High temperature brittle rupture strain	clad temperature = 670 °C plastic strain = f (fluence) [7]		brittle mode fracture
C3	Burst pressure	rupture stress = f (clad temperature) [8]	transient increase of fission gas pressure	burst of the cladding tube
C4	melting of unrestructured fuel	onset of melting of unrestructured fuel [9]		
C5	fuel melt fraction	melt fraction = 0.30 [10]		

Failure rip length: 5 cm
Fuel particle radius: 117 μ (instantaneous fragmentation)
Inertial length for ejection process: 10 cm

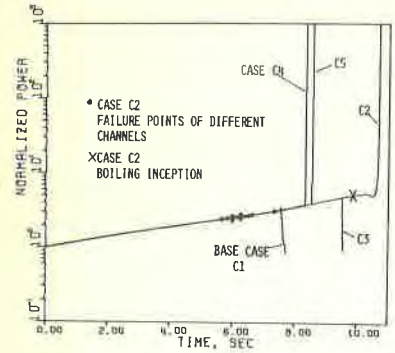

Fig. 4: Power vs. Time with Different Failure Criteria

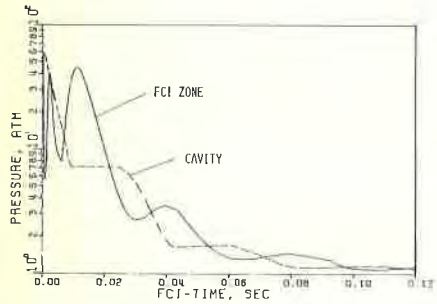

Fig. 6: FCI Zone and Cavity Pressure in CH10 (Case C1)

Tab.III: Results for 0.15 $/sec ramp accident with 1% rupture strain criterion

		Dim.	Base Case
Failure Point	Time	sec	7.54
	Normalized Power	-	3.30
	Net Reactivity	$	0.377
Conditions of Channel 10 at Failure	Peak Fuel Melt Fraction	%	10.1
	Failure Position	% Act.Height	61
	Failure Rip Length	cm	5
	Cavity Throat Area	cm^2	0.055
	Cavity Pressure	atm	58
FCI Results for Channel 10	Maximum Single Phase Pressure	atm	80
	Start of Phase 2	msec	8.2
	Percentage of Molten Fuel Ejected before Phase 2	%	40
	Peak Sodium Vapour Pressure	atm	65
	Maximum Fuel to Sodium Mass Ratio	-	2.9
	Start of Fuel Temp-out	msec	21
Integral Results	Peak Normalized Power	-	3.73
	FCI-Time at Peak Power	msec	15
Switch off Point (Normalized Power Returns to SS Power)	Time	sec	7.71
	FCI - Time	msec	163
	Net Reactivity and Ramp	$ $/sec	-0.760 -2.7
	Void Reactivity and Ramp	$ $/sec	0.066 +0.7
	Temp-out Reactivity and Ramp	$ $/sec	-1.160 -3.7
	Doppler Reactivity and Ramp	$ $/sec	-0.820 -2.2

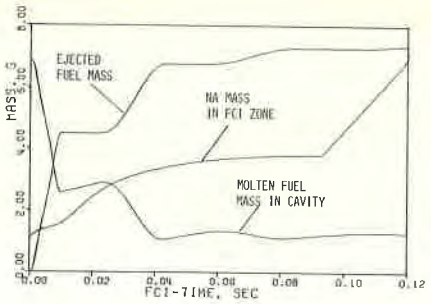

Fig. 5: Molten Fuel and Sodium Mass for FCI in CH10 (Case C1)

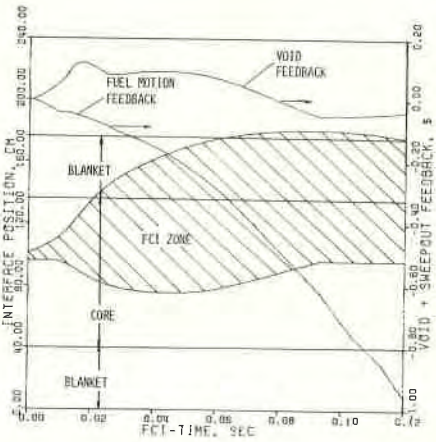

Fig. 7: FCI Zone Expansion and Resulting Feedbacks from CH10

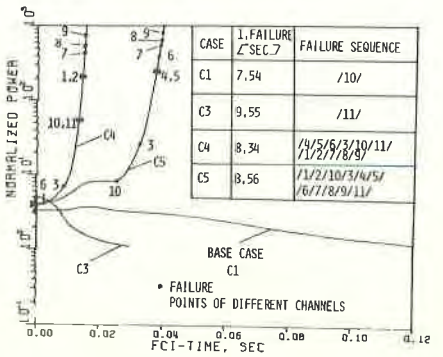

CASE	1.FAILURE [SEC]	FAILURE SEQUENCE
C1	7.54	/10/
C3	9.55	/11/
C4	8.34	/4/5/6/3/10/11/ /1/2/7/8/9/
C5	8.56	/1/2/10/3/4/5/ /6/7/8/9/11/

Fig. 8: Power VS. Time after Failure with Different Failure Criteria

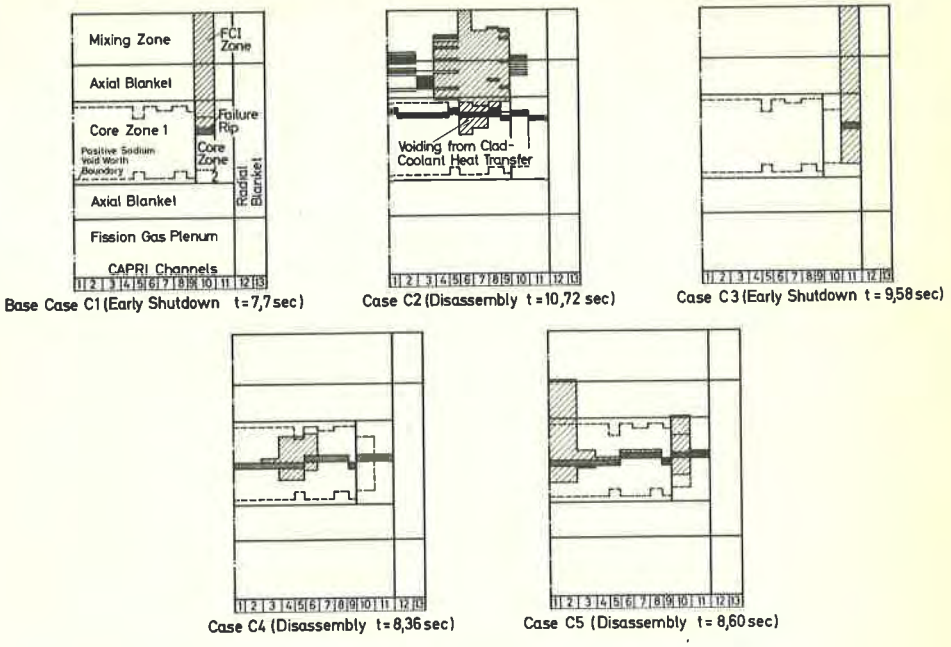

Fig. 9: Failure Positions and FCI-Zone and Voiding Patterns for Different Failure Criteria

Tab.IV: Comparison of accident sequence for different failure criteria

		Dim.	Base Case C1	Case C2	Case C3	Case C4	Case C5
First Failure	Time	sec	7.54	5.67	9.55	8.34	8.56
	Channel	-	10	6	11	4	1
	Cavity Pressure	atm	58	37	950	80	100
	Peak Melt Fraction	%	10	0	30	21	30
Failure Sequence	Channels	-	10	/6/5/1/4/7/8/ /3/10/2/9/11/	11	/4/5/6/3/10/ /11/1/2/7/8/9/	/1/2/10/3/4/ /5/6/7/8/9/11/
Core Voiding	Mechanism	-	Fission Gas Rel + FCI	Fission Gas Rel. + Clad-Coolant Heat Transfer	Fission Gas Release + FCI		
Fuel Motion	Dominant Feedback from:	-	Fuel Sweepout	No Fuel in Coolant Channel	Fuel Sweepout	Fuel Injection by Pressure Rise in Cavity	
Accident Termination	Mechanism	-	Early Shutdown	Disassembly	Early Shutdown	Disassembly	